The Journal of Engineering

WILEY

The Institution of Engineering and Technology

ORIGINAL RESEARCH OPEN ACCESS

Soft Open Points for Optimising Flexibility Exploitation in Power Distribution Networks

Sara Carcangiu | Gianni Celli | Mansoor U. M. Parehar | Fabrizio Pilo

Department of Electrical and Electronic Engineering, University of Cagliari, Cagliari, Italy

Correspondence: Gianni Celli (gcelli@unica.it)

Received: 5 March 2026 | **Revised:** 9 April 2026 | **Accepted:** 13 April 2026

ABSTRACT

Soft open points (SOPs) are installed in place of normally open tie switches, enabling controlled power exchange between adjacent feeders, typically to improve power quality in distribution networks. The main novelty of the paper is to consider this device a valuable solution for enabling the exploitation of the flexibility provided by distributed energy resources (DERs). A linear-programming operational planning framework is presented to quantify the value of coordinating SOPs with DERs for flexibility-oriented operation of distribution networks. The model optimises renewable generation curtailment and demand response along with SOP terminal active/reactive setpoints. Network adequacy and security are guaranteed through sensitivity-based linearised technical constraints around a forecast operating point, under steady and emergency network configurations. The N − 1 assessment applies a practical restoration policy that tests available network reconfiguration options and selects the one that reduces the load not served. In the post-fault topology, one SOP operates as a closed-tie switch to restore supply while keeping other devices controllable. The methodology is applied to a realistic Italian MV network and evaluated across monthly load and generation profiles. The proposed formulation provides a scalable and interpretable tool for assessing how SOP coordination impacts flexibility, procurement needs and security-constrained operating costs.

1 | Introduction

The ongoing electrification of end-use sectors and the accelerated deployment of renewable energy sources (RES) are profoundly reshaping the operation of medium-voltage (MV) distribution networks. Systems originally designed for largely unidirectional power flows are increasingly required to accommodate inverter-interfaced generation, bidirectional exchanges and growing operational variability driven by the simultaneous growth of photovoltaic (PV) installations, electric vehicles, and heat pumps [1, 2]. This evolution exacerbates well-known technical constraints: voltage rise at feeder ends under high PV penetration, thermal congestion on critical branches, three-phase unbalance under asymmetric loading, and a progressive reduction in the hosting capacity available for additional distributed energy resources (DERs). Large-scale studies and technical reports indicate that, without structural and operational innovations, these issues may limit the effective contribution of distribution grids to the energy transition while increasing operational complexity and costs [1, 2].

Flexibility services from distributed resources are therefore becoming a practical operational lever for distribution system operators (DSOs). In day-ahead operation, DSOs can schedule flexibility to mitigate anticipated voltage and current limit violations by curtailing RES injections, activating demand response, or demanding support from storage devices, provided that adequate controllable capacity is available in the affected electrical area [1, 2]. However, MV networks are commonly operated radially, which inherently restricts corrective actions: flexibility located outside the electrically influential feeder area may have limited or no impact on the violated constraints. As a result, the pool of

eligible flexibility can be narrow, and DSOs may face significantly higher operational costs or extensive PV curtailment, particularly in the most constrained feeders [2, 3].

Power-electronic devices such as soft open points (SOPs) offer an additional degree of controllability without requiring steady-state meshed operation. SOPs are typically implemented as back-to-back voltage source converters (VSCs) installed at normally open tie points between adjacent feeders, enabling controllable active power exchange and independent reactive power support at both terminals. Since the early development of SOP-like distribution-interconnection devices such as Siemens' SIPLINK [4], SOPs have attracted extensive research attention and are now recognised as a key enabling technology for active distribution networks. Comprehensive overviews of SOP technology, including topologies, control structures, benefit quantification indices, and worldwide industrial deployments, confirm that the field has matured significantly over the past decade [5, 6].

The operational benefits of SOPs have been widely investigated. Early studies demonstrated significant reductions in active power losses and improvements in feeder load balancing and voltage profiles, showing that a single SOP can achieve loss reductions comparable to full network reconfiguration [7]. Subsequent work formalised the SOP operating region using Jacobian-based sensitivity analysis, quantifying the trade-offs among voltage profile improvement, line utilisation balancing and energy loss minimisation under varying load and generation conditions [8]. The role of SOPs in increasing RES hosting capacity and mitigating overvoltage constraints has been extensively documented, with optimisation-based studies highlighting the trade-offs among hosting capacity, network losses, and deployment cost [9–11].

From a planning perspective, optimal siting and sizing of SOPs, frequently combined with network reconfiguration, have been formulated as mixed-integer, second-order cone, or metaheuristic optimisation problems [3, 9, 10, 12, 13]. Under unbalanced or uncertain operating conditions, three-phase SOP models and uncertainty-aware planning approaches have been proposed to mitigate voltage unbalance and reduce losses [14, 15]. The simultaneous optimisation of SOP placement and open-switch positions has been shown to outperform sequential approaches, yielding superior loss reductions [10].

Advances in SOP topology have further expanded operational capabilities beyond the two-terminal back-to-back architecture. Multi-terminal VSC configurations enable the simultaneous interconnection of three or more feeders, increasing the degrees of freedom available to the network operator [5, 16]. Hybrid multi-terminal SOPs, in which each converter leg is paired with feeder selector switches, have been shown to improve converter utilisation compared with equally sized conventional multi-terminal SOPs [16]. Phase-changing multi-terminal SOPs, modelled via semidefinite programming relaxation, provide additional flexibility for three-phase imbalance mitigation in unbalanced active distribution networks [17]. The integration of energy storage systems with SOPs, either co-deployed in planning or co-optimised in operation, enables the simultaneous exploitation of spatial and temporal flexibility, with joint configurations significantly reducing load shedding costs compared to standalone installations [18–22].

A substantial and growing strand of the literature focuses on SOP-assisted fault recovery and resilience enhancement. Under fault conditions, SOPs can support service restoration by facilitating the resupply of non-faulted sections and, in suitable configurations, the formation of self-sufficient microgrids with local generators [23, 24]. Two-stage restoration frameworks that coordinate SOPs with controllable distributed generation have demonstrated improved restoration performance compared to conventional methods [25]. Multi-period cooperative models that jointly optimise repair scheduling and network restoration with SOP control mode switching have been validated on large-scale systems [26]. The coordinated deployment of SOPs and remote-controlled switches for resilience improvement, formulated as a mixed-integer second-order cone programme over multiple recovery stages, has been shown to yield favourable resilience-cost trade-offs [27]. The role of SOPs in enhancing resilience against extreme weather events and cyberattacks, through robust optimisation and tri-level defender–attacker–defender models, respectively, has also been recently addressed, further confirming the versatility of the technology [18, 20].

Despite this broad and rapidly expanding body of work, the quantification of SOP value as a flexibility enabler in the context of DSO day-ahead procurement planning remains insufficiently addressed in the literature. Existing studies predominantly optimise SOP operation to minimise network losses [7, 8], improve voltage profiles or hosting capacity [9–11], or maximise load restoration following fault events [23–27]. In these formulations, the SOP is treated as a controllable device that improves network performance metrics; by contrast, the associated cost of flexibility services from DERs required to maintain technical feasibility is generally not the primary objective nor the main quantity being minimised.

In radially operated MV networks, however, one of the key operational challenges for DSOs is flexibility procurement: when voltage or thermal limits are violated, corrective actions must be contracted and activated from DER owners at a cost. In this context, the value of the SOP lies in its ability to couple adjacent feeders, thereby enlarging the set of electrically effective resources, increasing competition among them, and reducing the volume and cost of flexibility services that must be procured. This procurement-oriented perspective, which aligns directly with DSO decision-making in day-ahead operation, has received limited explicit attention in the existing literature. Furthermore, while several works address SOP operation or deployment under faulted and post-contingency conditions [23–27], they do not explicitly quantify the security-driven procurement envelope that defines the contracted flexibility and SOP reactive capability required to ensure feasibility across the set of credible single-branch outages considered in the $N-1$ assessment.

Building on the linear programming (LP)-based operational planning framework proposed in [28], which co-optimised SOP setpoints and flexibility activation on a realistic Italian MV network, this paper extends the formulation to enable the simultaneous operation of multiple two-terminal SOPs while preserving linearity and interpretability. The main contributions of this paper are (i) a linear-programming operational-planning framework that co-optimises the setpoints of multiple two-terminal SOPs together with RES curtailment and demand

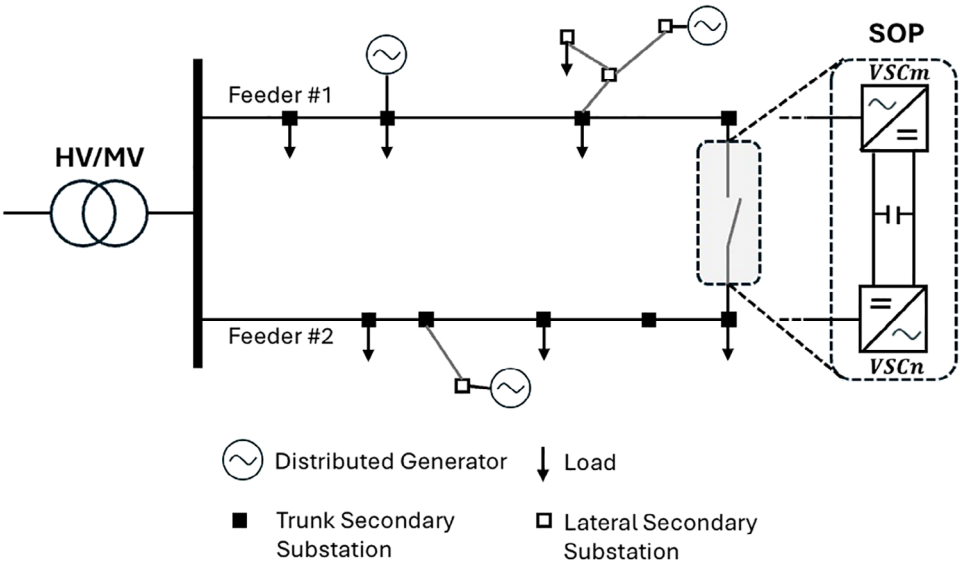

FIGURE 1 | Schematic representation of a two-terminal SOP installed between two MV feeders.

response, explicitly treating SOPs as controllable devices that expand the set of electrically effective flexibility resources in radial MV networks; (ii) a practical N − 1 assessment workflow that integrates a restoration screening policy into the day-ahead planning process, enabling the quantification of security-driven procurement envelopes; and (iii) a transparent procurement-oriented quantification of SOP value at annual scale on a realistic Italian MV network, including a comparison between single-and multi-SOP deployment under ordinary and emergency operating conditions. The focus on two-terminal back-to-back SOPs is deliberate: this architecture remains the most established industrial configuration, while extending the proposed framework to multi-terminal and storage-integrated SOP solutions is left for future work. Also, the inclusion into the operational planning objective function of only two simple flexibility services (generation curtailment and demand response) is intentional: to highlight and isolate the effect of SOP on flexibility procurement cost. Coordination with additional flexibility resources (e.g., storage devices) and network flexibility devices (e.g., on-load tap changers) will be developed as the research progresses.

The paper is organised as follows. Section 2 presents the SOP model and its LP-compatible linearisation; Section 3 formulates the operational planning problem; Section 4 describes the emergency assessment workflow; Section 5 introduces the case study and simulation setup; Section 6 reports and discusses the results; and Section 7 concludes the paper.

2 | Soft Open Point Modelling

A two-terminal SOP is typically realised by two VSCs connected in a back-to-back configuration, replacing a normally open mechanical tie switch between adjacent MV feeders. Each converter is typically interfaced to the AC network via a coupling transformer, and both converters share a common DC link (Figure 1). This architecture enables independent reactive power support at the two terminals while managing the active power exchanged between the feeders. In steady state, the SOP can be modelled as controllable power injections at its terminal buses $(P_m^{\mathrm{SOP}}, Q_m^{\mathrm{SOP}}, P_n^{\mathrm{SOP}}, Q_n^{\mathrm{SOP}})$.

Terminal reactive powers are independently controllable within converter limits. Terminal active powers must satisfy an active-power balance that accounts for conversion losses. Denoting by $P_{\mathrm{loss},m}^{\mathrm{SOP}}$ and $P_{\mathrm{loss},n}^{\mathrm{SOP}}$ the losses of the two converters, the balance is calculated in (1).

$$P_m^{\mathrm{SOP}} + P_n^{\mathrm{SOP}} + P_{\mathrm{loss},m}^{\mathrm{SOP}} + P_{\mathrm{loss},n}^{\mathrm{SOP}} = 0 \tag{1}$$

A common nonlinear representation expresses losses as proportional to the apparent power

$$\begin{aligned} P_{\mathrm{loss},m}^{\mathrm{SOP}} &= \alpha_{\mathrm{loss},m}^{\mathrm{SOP}} \times \sqrt{\left(P_m^{\mathrm{SOP}}\right)^2 + \left(Q_m^{\mathrm{SOP}}\right)^2} \\ P_{\mathrm{loss},n}^{\mathrm{SOP}} &= \alpha_{\mathrm{loss},n}^{\mathrm{SOP}} \times \sqrt{\left(P_n^{\mathrm{SOP}}\right)^2 + \left(Q_n^{\mathrm{SOP}}\right)^2} \end{aligned} \tag{2}$$

where $\alpha_{\mathrm{loss}}^{\mathrm{SOP}}$ is the loss coefficient. To reduce computational complexity in linear or piecewise-linear formulations, losses are approximated as proportional to the magnitude of active power [6]

$$\begin{aligned} P_{\mathrm{loss},m}^{\mathrm{SOP}} &= \alpha_{\mathrm{loss},m}^{\mathrm{SOP}} \times \left|P_m^{\mathrm{SOP}}\right| \\ P_{\mathrm{loss},n}^{\mathrm{SOP}} &= \alpha_{\mathrm{loss},n}^{\mathrm{SOP}} \times \left|P_n^{\mathrm{SOP}}\right| \end{aligned} \tag{3}$$

Finally, each terminal is constrained by its apparent power rating

$$\begin{aligned} \sqrt{\left(P_m^{\mathrm{SOP}}\right)^2 + \left(Q_m^{\mathrm{SOP}}\right)^2} &\le S_m^{\mathrm{SOP}} \\ \sqrt{\left(P_n^{\mathrm{SOP}}\right)^2 + \left(Q_n^{\mathrm{SOP}}\right)^2} &\le S_n^{\mathrm{SOP}} \end{aligned} \tag{4}$$

where S_m^{SOP} and S_n^{SOP} are the rated apparent powers of the two VSC terminals.

2.1 | LP-Compatible SOP Linearisation

The operational planning formulation adopted in this work relies on LP for computational efficiency and scalability; however, the SOP model described above is nonlinear due to the absolute values in (3) and the quadratic constraint in (4). Moreover, the active and reactive powers exchanged at each SOP terminal are free variables, i.e., they can be both positive and negative.

By introducing two auxiliary variables for each original free variable and the following additional constraints, the absolute value can be easily linearised, and the LP problem can be written only in terms of non-negative variables:

$$\left|P_{s,m}^{\mathrm{SOP}}\right| = P_{s,m}^{\mathrm{SOP}^+} + P_{s,m}^{\mathrm{SOP}^-} \tag{5}$$

$$P_{s,m}^{\mathrm{SOP}} = P_{s,m}^{\mathrm{SOP}^+} - P_{s,m}^{\mathrm{SOP}^-}$$

$$Q_{s,m}^{\mathrm{SOP}} = Q_{s,m}^{\mathrm{SOP}^+} - Q_{s,m}^{\mathrm{SOP}^-}$$

$$P_{s,m}^{\mathrm{SOP}^+} \geq 0\,;\; P_{s,m}^{\mathrm{SOP}^-} \geq 0\,;\; Q_{s,m}^{\mathrm{SOP}^+} \geq 0\,;\; Q_{s,m}^{\mathrm{SOP}^-} \geq 0$$

where index s refers to the generic SOP installed in the network, and m is the bus to which one converter of the sth SOP is connected.

Considering (5), SOP converter losses can be approximated with the following model:

$$P_{\mathrm{loss},s,m}^{\mathrm{SOP}} = \alpha_{\mathrm{loss},s,m}^{\mathrm{SOP}} \times \left(P_{s,m}^{\mathrm{SOP}^+} + P_{s,m}^{\mathrm{SOP}^-}\right) \tag{6}$$

and the SOP active power balance is linearised as

$$\left(P_{m}^{\mathrm{SOP}^+} - P_{m}^{\mathrm{SOP}^-}\right) + \left(P_{n}^{\mathrm{SOP}^+} - P_{n}^{\mathrm{SOP}^-}\right) + \alpha_{\mathrm{loss},m}^{\mathrm{SOP}} \times \left(P_{m}^{\mathrm{SOP}^+} + P_{m}^{\mathrm{SOP}^-}\right) + \alpha_{\mathrm{loss},n}^{\mathrm{SOP}} \times \left(P_{n}^{\mathrm{SOP}^+} + P_{n}^{\mathrm{SOP}^-}\right) = 0 \tag{7}$$

The converter capability constraint (4) couples active and reactive support through a circular boundary in the (P,Q) plane. An inscribed regular convex polygon with l edges can approximate this circular constraint. The coordinates of the generic polygon vertex c_k are expressed as (Figure 2)

$$\begin{aligned} x_k &= S_{rated}^{\mathrm{SOP}} \times \cos\left(\tfrac{2\pi}{l}k\right) \\ y_k &= S_{\mathrm{rated}}^{\mathrm{SOP}} \times \sin\left(\tfrac{2\pi}{l}k\right) \end{aligned} \tag{8}$$

Numbering the vertices sequentially in counterclockwise order, the equation of the directed edge $c_{k-1} \rightarrow c_k$ is given in (9).

$$(y_{k-1} - y_k)\,x - (x_{k-1} - x_k)\,y + x_k y_{k-1} - x_{k-1}\,y_k = 0 \tag{9}$$

If the generic point (x, y) does not belong to the edge, (9) represents the double of the oriented area of the triangle defined by points (x_{k-1}, y_{k-1}), (x_k, y_k), and (x, y). When the generic point (x, y) lies to the left of the edge, the area is negative; otherwise, it is positive. By exploiting this rule (derived from the shoelace formula), a generic point lies inside the polygon when (9) is negative for all edges.

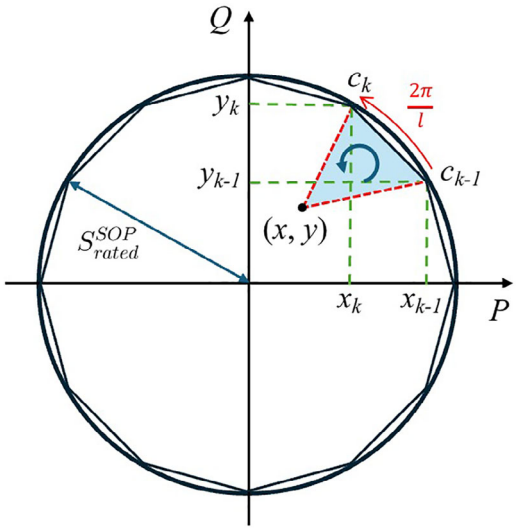

FIGURE 2 | Linearisation of quadratic constraint for SOP operation through an inscribed regular polygon.

For the setpoint at time t of the converter installed on bus m of the sth SOP, by substituting (5) and (8) into (9) and after some algebraic manipulation, the nonlinear constraint (4) can be replaced by the following set of l linear constraints:

$$\begin{aligned} &\left[\sin\left(\frac{2\pi\,(k-1)}{l}\right) - \sin\left(\frac{2\pi k}{l}\right)\right]\left(P_{s,m,t}^{\mathrm{SOP}^+} - P_{s,m,t}^{\mathrm{SOP}^-}\right) \\ &- \left[\cos\left(\frac{2\pi\,(k-1)}{l}\right) - \cos\left(\frac{2\pi k}{l}\right)\right] \\ &\left(Q_{s,m,t}^{\mathrm{SOP}^+} - Q_{s,m,t}^{\mathrm{SOP}^-}\right) + S_{rated,s}^{\mathrm{SOP}} \sin\frac{2\pi}{l} \leq 0\;\forall k = 1,\ldots,l \end{aligned} \tag{10}$$

The extension of (10), as for the whole mathematical formulation of the operational planning problem, to all the intervals used for discretising the optimisation time-horizon (e.g., the 24 h of a day-ahead horizon) is helpful to obtain a picture of the requested flexibility in a single calculation, and it will become compulsory when time-dependent energy resources are considered, such as storage devices (the next advancement of the research).

The greater the number of polygon edges (l), the more accurate the approximation, but the heavier the computational burden. Indeed, each SOP terminal adds $2lT$ inequality constraints (2 terminals $\times$ l sides $\times$ T time steps) to the mathematical formulation of the optimisation problem, so the constraint matrix grows linearly with l. The maximum geometric approximation error between the polygon and circular boundaries is the difference between the apothem and the radius, $\varepsilon_{\mathrm{geom}} = 1 - \cos(\pi/l)$, corresponding to 0.86% at $l = 24$. However, the impact on the objective function depends on whether the SOP capability constraint is active at the optimum, i.e., if the optimal solution lies on this boundary. A sensitivity analysis of the effect of l on both solution accuracy and computation time is reported in Section 6.5.

2.2 | SOP Setpoints Into the Linearised Network Model

SOP terminal setpoints are embedded into a linearised network model through sensitivity-based constraints around a base operating point. For each hour t, a power flow (PF) calculation provides the base vectors for nodal voltage magnitudes V_t^0 and branch current magnitudes I_t^0. Incremental control actions are collected into vectors ΔP_t and ΔQ_t, where ΔP_t includes RES curtailment, demand response, and SOP terminal active injections, while ΔQ_t includes SOP terminal reactive injections. The first-order approximation in (11) leads to the linear security constraints in (12) and (13).

$$\begin{aligned} V_t &\approx V_t^0 + S_{VP,t}\Delta P_t + S_{VQ,t}\boldsymbol{\Delta} Q_t \\ I_t &\approx I_t^0 + S_{IP,t}\Delta P_t + S_{IQ,t}\boldsymbol{\Delta} Q_t \end{aligned} \tag{11}$$

$$V^{\min} \le V_t^0 + S_{VP,t}\boldsymbol{\Delta} P_t + S_{VQ,t}\boldsymbol{\Delta} Q_t \le V^{\max} \tag{12}$$

$$I_t^0 + S_{IP,t}\boldsymbol{\Delta} P_t + S_{IQ,t}\Delta Q_t \le I^{\max} \tag{13}$$

S_{VP}, S_{VQ}, S_{IP} and S_{IQ} are sensitivity matrices derived from the base PF solution; $V^{\min}$ and $V^{\max}$ are the vectors of the nodal voltage limits (equal for bus), and $I^{\max}$ is the vector of the branch ampacities (dependent on conductor type and cross sections).

SOP actions enter (12) and (13) through their terminal injections, as described by the second and third equations in (5), ensuring fully linear integration of SOP controllability into the operational planning constraints.

3 | Operational Planning Problem Formulation

In a day-ahead setting, the DSO determines the least-cost combination of flexibility actions required to keep the network within voltage and thermal limits. Operational planning is formulated as an LP problem, with the objective function and all constraints linearised, as described for SOP. In the paper, only RES curtailment and demand response are considered as flexibility services from DERs, while battery energy storage systems (BESSs) are not included. However, the multi-period LP formulation is already defined over a 24-hour horizon to accommodate time-coupled energy-constrained resources such as BESSs. Apart from decision variables and charging/discharging limits, their inclusion shall require additional intertemporal constraints, such as state-of-charge balance equations.

The optimisation is solved over a day-ahead horizon of T hourly intervals. Let $\Delta P_{g,t}^{\mathrm{DG}} \ge 0$ be the curtailed active power of the RES unit $g \in \{1,\dots,N_G\}$ at hour t, and $\Delta P_{d,t}^{\mathrm{DR}} \ge 0$ the curtailed consumption of the demand–response participant $d \in \{1,\dots,N_D\}$ at hour t, where N_G and N_D are the numbers of RES and loads participating in flexibility plans. The control vectors are given in (14).

$$\boldsymbol{\Delta} P_t = \left[\boldsymbol{\Delta} P_t^{\mathrm{DG}};\, \boldsymbol{\Delta} P_t^{\mathrm{DR}};\, P_t^{\mathrm{SOP}}\right],\ \Delta Q_t = \left[Q_t^{\mathrm{SOP}}\right] \tag{14}$$

Here, P_t^{SOP} and Q_t^{SOP} stack the terminal setpoints of all active SOPs at the hour t. The number of SOP terminals is $N_T = 2N_{\mathrm{SOP}}$ when only two-terminal devices are considered.

The operational planning objective is to minimise the total cost of flexibility activation over the horizon while accounting for SOP conversion losses. The objective function is written as

$$\min_{\{\boldsymbol{\Delta} P_t, \boldsymbol{\Delta} Q_t\}} \sum_{t=1}^{T} \left(\sum_{g=1}^{N_G} c_g^{\mathrm{DG}}\, \boldsymbol{\Delta} P_{g,t}^{\mathrm{DG}} + \sum_{d=1}^{N_D} c_d^{\mathrm{DR}}\, \boldsymbol{\Delta} P_{d,t}^{\mathrm{DR}} + \sum_{m=1}^{N_T} c_{loss}\, P_{\mathrm{loss},m,t}^{\mathrm{SOP}} \right) \tag{15}$$

where c_g^{DG} and c_d^{DR} are the unit costs associated with RES curtailment and demand response, respectively, c_{loss} is the unit cost associated with SOP conversion losses, and $P_{\mathrm{loss},m,t}^{\mathrm{SOP}}$ is computed via (6).

For each hour t, voltage and current limits are enforced by substituting the control vectors into the linearised relationships (11), yielding constraints (12)–(13).

For each SOP s and hour t, SOP operation is constrained by the linear active-power balance (7), the loss model (6), and the polygonal capability constraints (10) at both terminals.

Flexibility actions are bounded by available offers

$$0 \le \boldsymbol{\Delta} P_{g,t}^{\mathbf{DG}} \le \Delta \bar{P}_{g,t}^{\mathbf{DG}}, \forall g, \forall t \tag{16}$$

$$0 \le \boldsymbol{\Delta} \boldsymbol{P}_{d,t}^{\mathbf{DR}} \le \boldsymbol{\Delta} \bar{P}_{d,t}^{\mathbf{DR}}, \forall d, \forall t \tag{17}$$

where $\Delta \bar{P}_{g,t}^{\mathbf{DG}}$ is the maximum curtailment that can be applied at hour t, typically limited by the forecasted RES injection, and $\Delta \bar{P}_{d,t}^{\mathbf{DR}}$ reflects the agreed load reduction capacity at hour t. These bounds preserve the physical and contractual limits of flexibility resources, preventing the LP from relying on infeasible control actions. It is important to note that in the paper, demand response flexibility is represented solely by load reduction (never by load increment); consequently, the two services cannot compete on technical grounds: generation curtailment is a "downward" service used to reduce overvoltage, while demand response is an "upward" service used to raise excessive undervoltage. Both can reduce overcurrent, but they are not used simultaneously to solve this situation; otherwise, the compensation effect between generation and load is lost.

4 | Emergency Assessment Workflow

This section describes the emergency assessment procedure adopted to quantify how the operational planning solution adapts to single-branch outages in radially operated MV distribution networks. When a post-fault reconfiguration must be created, the selected SOP changes its operation from "power flow mode control" (where the main objective is to provide the required exchange of active and reactive power for maintaining acceptable operating conditions) to "supply restoration mode control" (where the converter connected to the isolated subnetwork operates as a voltage source).

For each contingency, the procedure reconstructs the post-fault topology, evaluates the restoration benefit of limited reconfiguration actions, updates the set of available SOP devices consistently with the resulting network topology (i.e., those that are not providing the supply restoration service and can be controlled

to support the distribution system), and finally solves the operational planning problem of Section 3 on the supplied portion of the network. Non-supplied (isolated) graph components are accounted for through an interrupted-load indicator and are not credited with autonomous flexibility activation unless a restoration path is present.

Let $\mathcal{L}$ denote the set of branches in the base topology and let $\mathcal{C} \subseteq \mathcal{L}$ be the set of contingencies, consisting of all branches energised in the base operating state. For each contingency $c \in \mathcal{C}$, the post-fault switching state is obtained by opening branch c while keeping all other branch states unchanged. The resulting network graph is analysed to identify connected components (i.e., the connected subnetworks formed after the removal of the faulted branch). A component k is classified as supplied if it contains at least one primary substation (PS) (slack) bus, i.e.,

$$\mathcal{N}_k \cap \mathcal{N}_{\text{slack}} \neq \emptyset \tag{18}$$

where $\mathcal{N}_k$ is the bus set of the component k (i.e., the list of buses included in the k-th subnetwork) and $\mathcal{N}_{\text{slack}}$ denotes the set of slack buses representing the MV sources. Components that do not satisfy (18) are considered unsupplied for that contingency (isolated subnetwork) and contribute to the interrupted-load metric defined below.

Following component identification, an optional post-fault reconfiguration action based on normally open ties is evaluated. Let $\mathcal{T}$ be the set of normally open branches in the base configuration. For a given contingency c, candidate tie closures are tested by temporarily closing each $e \in \mathcal{T}$ (one at a time) and recomputing the connected components. Candidate closures that create a component containing more than one slack bus are discarded, as they would introduce meshed operation, which is typically avoided in MV systems and conflicts with the single-source structure assumed for protection coordination. The remaining candidates are ranked by the load-not-served (LNS) indicator, computed as the sum of forecasted active demand located in isolated components.

$$\text{LNS}(c, e) = \sum_{k\,:\,\mathcal{N}_k \cap \mathcal{N}_{\text{slack}} = \emptyset} \; \sum_{i \in \mathcal{N}_k} P_i^{\text{load}} \tag{19}$$

where P_i^{load} is the forecasted active load at bus i for the considered time step. The selected tie $e^\star$ for contingency c is the one that minimises $\text{LNS}(c, e)$ and yields a strict improvement with respect to the "no action" case. If no candidate closure improves the indicator, no tie is closed, and the post-fault topology remains as obtained by opening c. This situation corresponds to a fault on a lateral branch, resulting in an isolated subnetwork that cannot be resupplied.

The emergency topology resulting from the contingency and the (optional) tie closure determines SOP availability and modelling. An SOP device is included in the contingency LP model only when both its terminals belong to the same supplied subnetwork; if the contingency separates its terminals or places one terminal in a non-supplied component, the device is excluded from that optimisation. The SOP selected for emergency reconfiguration to provide the supply restoration service is treated as bypassed for the considered contingency, i.e., it is disregarded in the operational planning optimisation. All other SOPs that are entirely within supplied components remain controllable and are included in the LP model.

For each contingency c, after the topology and device set are established, the operational planning problem in Section 3 is solved on the supplied portion of the network. The network data are filtered to retain only the branches and the buses belonging to supplied components; loads and RES units are similarly filtered by bus membership. Base-point quantities and sensitivity matrices are recalculated for the specific contingency topology and operating condition, and the LP is solved to obtain contingency-specific flexibility activation and SOP terminal setpoints that satisfy voltage and thermal constraints at minimum cost. Components that are not supplied according to (18) are not optimised; since this work does not rely on storage resources and does not assume autonomous dispatch in islanded areas (intentional islanding operation), flexibility actions within non-supplied components are not credited unless a restoration path exists through the selected tie closure. Their forecasted loads, therefore, contribute to *LNS* and are reported as an interrupted load for the contingency.

The contingency assessment produces, for each $c \in \mathcal{C}$, (i) an LP solution for the supplied portion of the network and the associated objective value (flexibility exploitation from DERs), (ii) the corresponding SOP terminal setpoints for the devices available under that contingency topology, and (iii) the LNS indicator in (19). To support a procurement-oriented interpretation, contingency outcomes are aggregated using a security-driven worst-case criterion. For each flexibility activation variable and each SOP terminal setpoint, the required contracted capacity (or operational envelope) is defined as the maximum absolute activation observed across the contingency set (and across time steps when applicable). This aggregation yields requirements that are sufficient to cover all considered single-branch outages under the adopted switching policy, while preserving the transparency and computational efficiency of the LP-based planning framework. In complex urban networks, where the number of available tie connections is higher than in rural areas, DSOs may adopt multiple switching actions. This advanced network management has not been considered in the paper because it involves a nested optimisation with a consequent increment in computational complexity, thus jeopardising the proposed LP framework's scalability. This reconfiguration logic will be investigated in future work together with different reconfiguration's objective functions (e.g., availability maximisation of flexibility services).

5 | Case Study and Simulation Setup

An MV test case was constructed by merging selected portions of an existing Italian distribution network, and renewable generation was allocated to emulate operating conditions consistent with high-PV penetration scenarios. The resulting system is representative of a rural MV grid supplied by a PS and operated through two main feeders (Figure 3). The network includes 25 secondary substations and a maximum distance of 17.3 km from the PS to the farthest node. Loads represent a mix of residential, tertiary, and agricultural customers, with an overall nominal

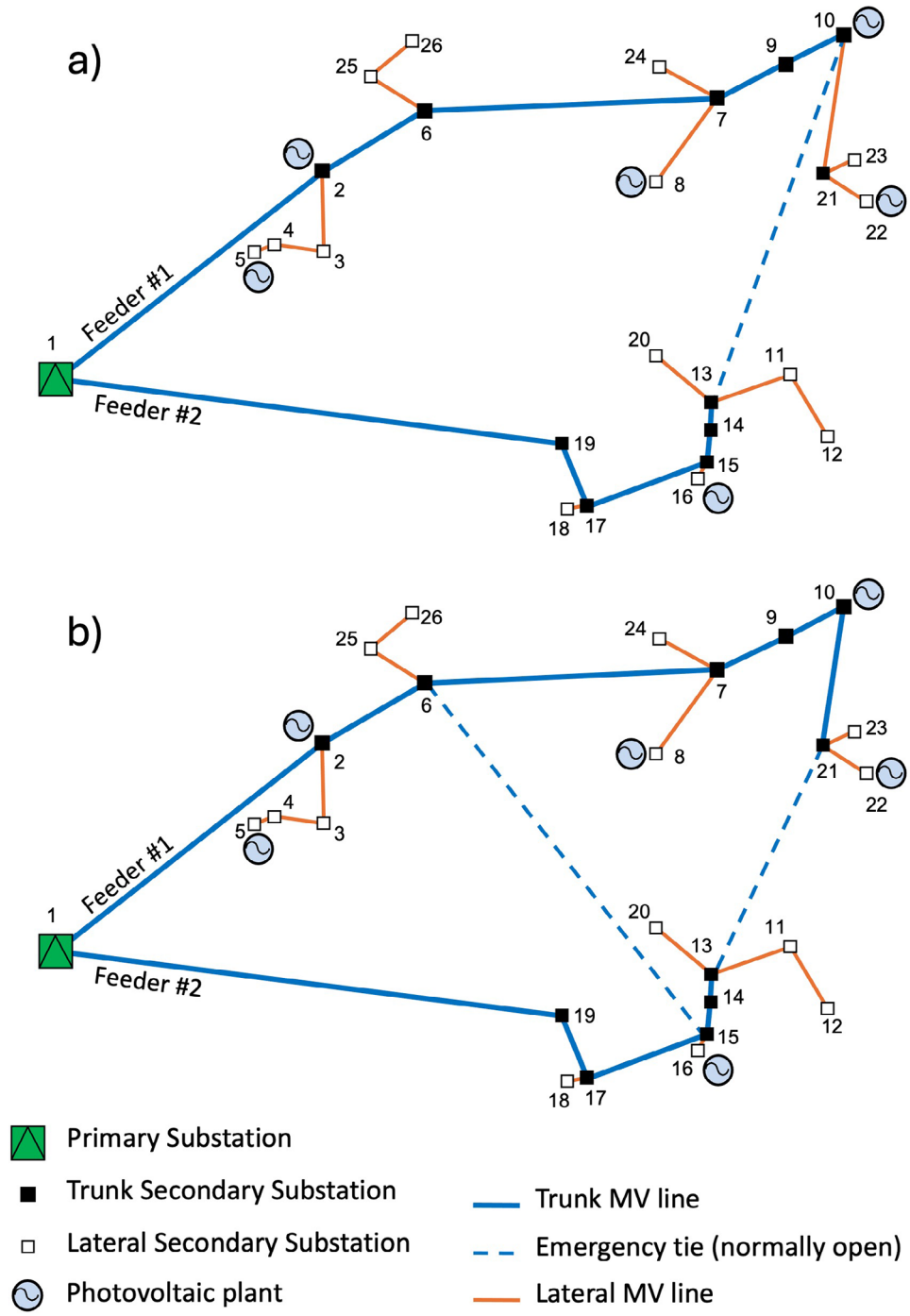

FIGURE 3 | Network topology: (a) Case A (single SOP) and (b) Case B (coordinated multi-SOP).

demand of approximately 1.7 MW and an evening peak typical of rural MV areas. Six PV plants are connected to the network, with individual capacities ranging from 0.8 to 1.5 MW. The total installed PV power is about 4.4 MW on feeder 1 and 1.2 MW on feeder 2. Under high-irradiance conditions, this generation mix produces voltage rise (and, in specific sections, power congestions) driven by high PV injections combined with comparatively low daytime demand. From a structural perspective, the system follows a typical Italian MV scheme with a trunk–lateral organisation: trunk nodes correspond to substations that can be resupplied through at least two alternative paths from the same PS (or, in general, from different supply points), whereas laterals are single-path branches connected to the trunk. In this framework, post-fault reconfiguration aims to restore the trunk supply by changing the switching state of normally open branches while maintaining protection-friendly operation.

Two alternative emergency-tie configurations are analysed on the same physical network to evaluate the performance of SOPs under different deployment scales. In both configurations, SOPs are installed exclusively on normally open emergency ties, replacing the corresponding mechanical switches. **Case A** (single SOP) considers one normally open tie interconnecting the two feeders between buses 10 and 13 (Figure 3a). This configuration

TABLE 1 | Case studies parameters.

Item	Case A	Case B
Simulation scope	Normal operation	Normal + N − 1 operation
Nominal line-to-line voltage	15 kV	
Thermal limit of emergency cable	140 A	
Emergency tie apparent-power limit	3.7 MVA	
Number of SOPs	1	2
SOP buses	(10, 13)	(6, 15); (21, 13)
SOP apparent power rating	1.0 MVA	
$\alpha_{\text{loss}}^{\text{SOP}}$	0.02	
Loss unit cost ($c_{l_{\text{oss}}}$)	0.3€/kWh	
Polygon edges (l)	24	

TABLE 2 | Operational constraints and flexibility cost parameters.

Parameter	Value
Minimum voltage magnitude, $V^{\min}$	0.95 p.u.
Maximum voltage magnitude, $V^{\max}$	1.05 p.u.
Branch current limit, $I^{\max}$	From network data (ranging from 105 to 330 A)
RES curtailment unit cost, c_g^{DG}	0.30987€/kWh
Demand response unit cost, c_d^{DR}	0.30987€/kWh
Max PV curtailment (per generator, per hour)	$1 \cdot P_{g,t}^{G}$
Max DR reduction (per load, per hour)	$0.4 \cdot P_{d,t}^{L}$
Hourly intervals	24
Voltage and current slack variables added to constraints to prevent infeasibility	$s_{V,t}^{\min}$, $s_{V,t}^{\max}$, $s_{I,t}$
Slack penalty weights	10^{10}
Number of days represented by the simulated day-type/month	From input

is examined only under normal operating conditions. It is used to highlight the benefits an SOP can bring to DER flexibility exploitation by providing volt/VAR support to the critical feeder and, when conditions allow, enabling controlled feeder-to-feeder active power exchange. **Case B** (coordinated multi-SOP) considers two normally open ties interconnecting the feeders between buses 6–15 and 21–13 (Figure 3b). This configuration is examined under normal and N−1 operation, and it is used to quantify the annual impact of coordinated multi-SOP operation and the security-driven procurement envelope.

The network nominal line-to-line voltage is $V_n = 15\,\text{kV}$. In the case study, the ampacity of the emergency conductors is $I^{\max} = 140\,A$, which implies an upper bound on the transferable apparent power through the interconnection of $S^{\max} = \sqrt{3} \cdot V_n \cdot I^{\max} \simeq 3.7\,\text{MVA}$. This value represents an upper ceiling for any controllable exchange on that link. In the simulations, a rated apparent power of $S^{\text{SOP}} = 1\,\text{MVA}$ is assigned to each SOP converter, which remains well below the cable ampacity and is consistent with a conservative converter sizing intended to capture the effect of limited but dispatchable inter-feeder exchange. The SOP loss coefficients and polygonal capability approximation settings are summarised in Table 1.

The operational planning problem is solved over a day-ahead horizon of $T = 24$ hourly intervals. The assessment is repeated across all months of the year using the available daily load and PV generation profiles, which capture seasonal and weekly (weekday, Saturday, and Sunday/holiday) variability of both demand and RES generation. Therefore, a whole year is represented by 36 typical daily profiles. For every hour t of each profile, a PF solution is computed on the radial operating topology to obtain the initial state (V_t^0, I_t^0) and the sensitivity coefficients used in the linearised constraints of Section 3. The LP then determines the least-cost combination of flexibility services and SOP terminal setpoints that restores feasibility with respect to voltage and thermal limits.

Voltage bounds and branch current limits adhere to typical DSO practices for MV networks and are listed in Table 2. Standard EN 50160 specifies voltage-quality limits at network user terminals, with acceptable deviations typically summarised as $V_n \pm 10\%$ under normal operation, according to the standard's time-based criteria. In this study, the narrower range of 0.95 to 1.05 p.u. is not set as a direct regulatory limit for the MV network but serves as a conservative DSO-focused planning assumption. This approach accounts for the practical need to preserve part of the overall voltage margin for the LV network downstream of the MV/LV transformers. Consequently, voltages below 0.95 p.u. and above 1.05 p.u. are deemed unacceptable in the MV operational planning context.

The unit flexibility cost adopted in the paper is calibrated from representative bid data derived from the PicoFlex market analysis available in the literature [29]. The same value is intentionally assigned to RES curtailment and demand response to isolate the effect of SOP coordination from the relative pricing of the two flexibility products.

The emergency (N−1) analysis follows the workflow described in Section 4 and is performed only for Case B. Each normally energised branch is faulted one at a time. The post-fault connectivity is then analysed, and a restoration action is considered by testing the closure of normally open ties. At most one tie closure

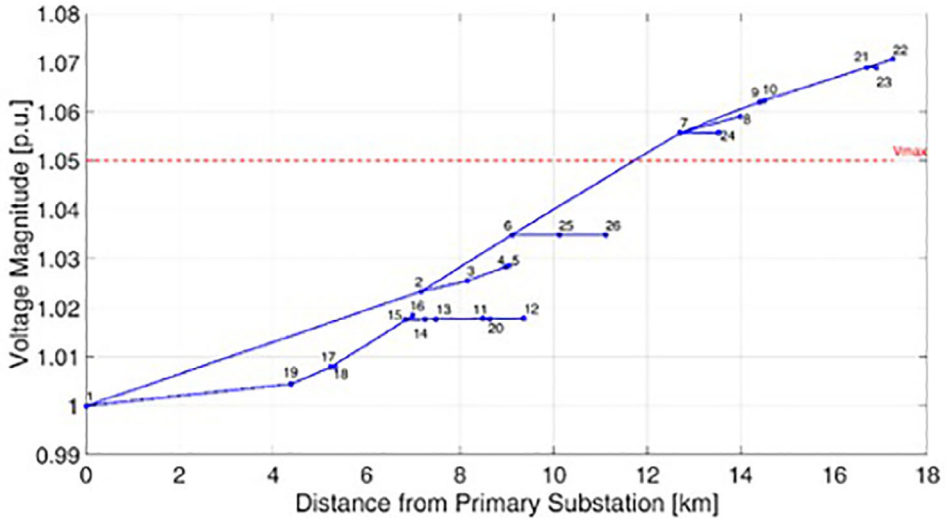

FIGURE 4 | Voltage profiles along the two feeders at 14:00 of a sunny summer day.

is applied per fault, selected only when it strictly reduces the interrupted load according to the LNS criterion. SOP availability is then updated consistently with the post-fault topology: SOPs are dispatched only when both terminals lie in the supplied portion of the network. If a normally open branch hosting an SOP is closed for restoration, the SOP on that link is treated as bypassed for that fault scenario, while the remaining SOP(s) remain controllable.

The proposed methodology has been implemented in a Python-based toolchain that integrates PF calculations via calls to the external OpenDSS software and an LP solver for the operational planning problem assessment. When an emergency configuration must be examined, the procedure reconstructs the post-fault topology, selects available restoration actions, updates the set of available SOPs, and resolves the LP on supplied components.

For every network configuration, the tool stores the flexibility activation and SOP setpoints together with network performance indicators (e.g., post-dispatch voltage margins and branch loading). When all configurations have been examined, the optimal amount of flexibility a DSO should purchase in the day-ahead market is the maximum flexibility requested for each DER in each hour across all the possible N configurations. By repeating this procedure for each daily profile and weighting the relative procurement cost by the number of days the specific typical profile occurs in the year, the annual cost of exploiting flexibility from DERs is estimated.

6 | Results and Discussion

This section presents the primary outcomes of the proposed operational planning tool, with particular emphasis on how the scale of SOP deployment affects flexibility procurement and network feasibility. Results are presented by distinguishing the two configurations introduced in Section 5. Case A (single SOP) is used to examine the underlying physical mechanisms and demonstrate, under clear representative conditions, how a two-terminal SOP can relieve PV-driven overvoltage through coordinated active and reactive power exchange. Case B (coordinated multi-SOP) extends the analysis to a full-year assessment under ordinary operation and to a security-oriented N − 1 evaluation, where procurement is defined via a worst-case envelope across single-branch outages. Costs refer to the objective value of Section 3 computed on the representative day and annualised using the number of occurrences of each day type in each month.

Throughout this section, two cost indicators are used: the representative-day objective value $C^{\text{day}}_{\text{flex}}$[€], i.e., the flexibility cost returned by the 24-hour OPF for a given month/day-type, and the corresponding annualised contribution $C^{\text{ann}}_{\text{flex}}(m,d) = C^{\text{day}}_{\text{flex}}(m,d)\,N_{m,d}$[€], where $N_{m,d}$ is the number of occurrences of that day-type within the month m.

6.1 | Case A – Single-SOP in Ordinary Operation

Case A is intended to highlight the core SOP value proposition in its most interpretable form, namely, the ability to provide both reactive voltage support and controlled feeder-to-feeder exchange through a normally open interconnection. Under high-irradiance conditions, the network exhibits the classical voltage-rise pattern of PV-dominated MV feeders: voltage increases with distance from the PS, and the most remote sections of the critical feeder may exceed the technical limit $V^{\max} = 1.05$ p.u., as illustrated in Figure 4.

If day-ahead forecasts warn the DSO about this possibility, it must activate remedial actions to prevent the critical scenario (e.g., network reconfiguration) or be prepared to address possible contingencies by leveraging local flexibility. This second option is discussed, with or without SOP.

When SOPs are not available, only local DER flexibility can be used. In this setting, the LP predominantly relies on PV active-power curtailment at the most electrically effective buses of the critical feeder, because curtailment directly reduces net injections and therefore mitigates voltage rise. The DSO can exploit only

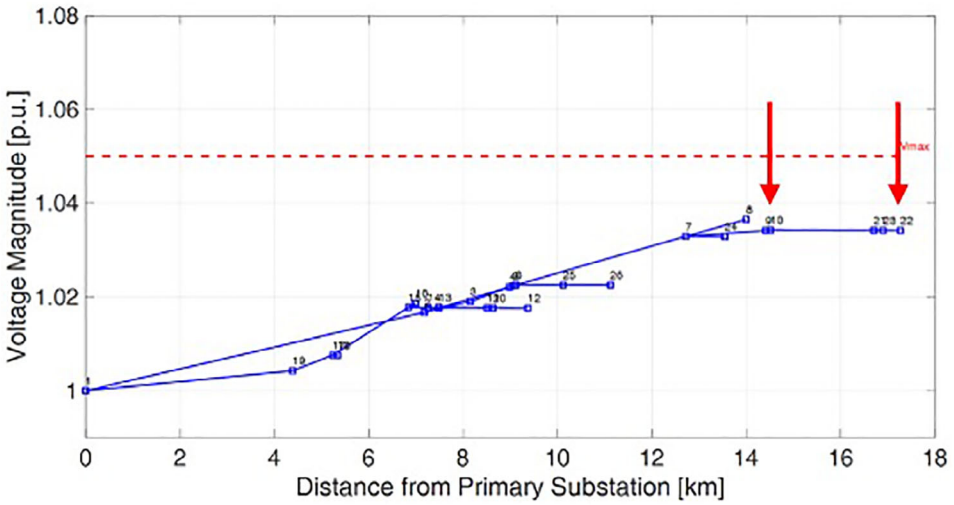

FIGURE 5 | Voltage profile correction at 14:00 by curtailing generation at nodes 10 and 22.

TABLE 3 | Flexibility required to solve overvoltage contingencies in feeder 1.

	Generation curtailment				
PV node	**12:00**	**13:00**	**14:00**	**15:00**	**16:00**
10	—	—	11%	—	—
22	14%	76%	95%	76%	14%

the flexibility offered by DERs (generators and responsive loads) connected to the feeder with the voltage regulation issue. The emergency connection from nodes 10 and 13 is open, and the potential overvoltage on feeder 1 can be solved only by its local resources (generators at nodes 2, 5, 8, 10, and 22). The OPF calculations identify generation curtailment of PV plants connected to nodes 22 (mainly) and 10 (marginally) as the optimal actions, as summarised in Table 3 and shown in Figure 5.

Consequently, the total flexibility that the DSO must purchase for a secure day-ahead network operation corresponds to approximately 3,000 kW of curtailed generation between 12:00 and 16:00, costing €21.4 k€.

With the SOP enabled on the emergency tie, the correction mechanism undergoes a qualitative change. As shown in Figure 6, the emergency mechanical switch between nodes 10 and 13 (normally open) is assumed to be replaced by a SOP. The SOP can absorb reactive power at the critical terminal to locally reduce voltage sensitivity and, when the adjacent feeder has sufficient headroom, transfer active power across feeders to redistribute net injections. Specifically, on node 10, the SOP operates as an inductor, absorbing reactive power for all 5 h during the overvoltage limit violation. This contribution avoids resorting to generation curtailment in two of these five hours, thereby reducing the exploitation of this service in the remaining three (Table 4).

Moreover, the SOP provides downward service by absorbing active power from the first feeder and injecting it into the

TABLE 4 | Flexibility exploitation and SOP operation. Active and reactive powers absorbed by the SOP converter are assumed to be positive (and negative when injected).

Flexibility resources		**12:00**	**13:00**	**14:00**	**15:00**	**16:00**
GC	PV_{10}	—	—	—	—	—
	PV_{22}	—	19%	44%	19%	—
SOP [kW, kVar]	P_{10}^{SOP}	—	296	296	296	—
	P_{13}^{SOP}	—	−283	−283	−283	—
	Q_{10}^{SOP}	146	386	386	386	144
	Q_{13}^{SOP}	—	—	—	—	—

second one. The second feeder shows an increase in its voltage profile without causing new constraint violations. The voltage profile remains below the maximum technical limit (see voltage profiles in Figure 7). Therefore, the SOP does not provide any reactive power support for the second feeder. The combination of these two actions allows reducing the flexibility purchased by 70%, achieving a total request for generation curtailment availability of around 850 kW (from 13:00 to 15:00), at a cost of 6.5 k€.

To expand the analysis of the SOP behaviour, a second case was studied by forcing a technical constraint violation also in the second feeder, where the maximum voltage limit was artificially reduced to 1.01 p.u. Simulating the two feeders independently (i.e., without considering the SOP), the amount of generation curtailment that the DSO should procure (7230 kW) and the corresponding relative cost (51.5 k€) are high. The PV at node 16 must be heavily curtailed during critical hours, as it is the only flexibility resource available along the second feeder. The presence of the SOP enables the combination of all resources, resulting in a reduced DSO cost to 11.9 k€. Together with reactive power support from the SOP, the required generation curtailment is significantly reduced (by 77%) by operating the converters to transfer active power from feeder 2 to feeder 1 and to absorb reactive power in both feeders (see Figure 8 and Table 5).

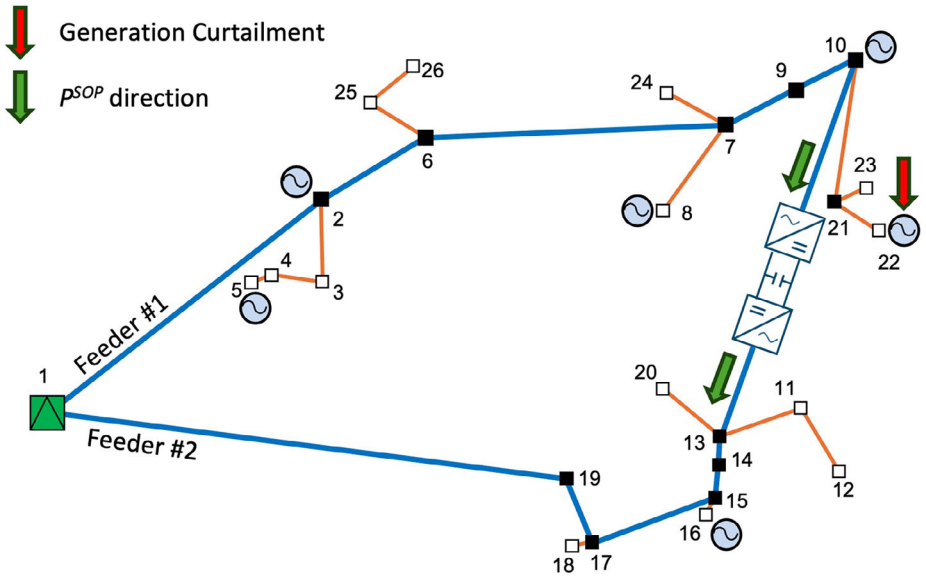

FIGURE 6 | Test case with the emergency mechanical switch between nodes 10 and 13 replaced by an SOP.

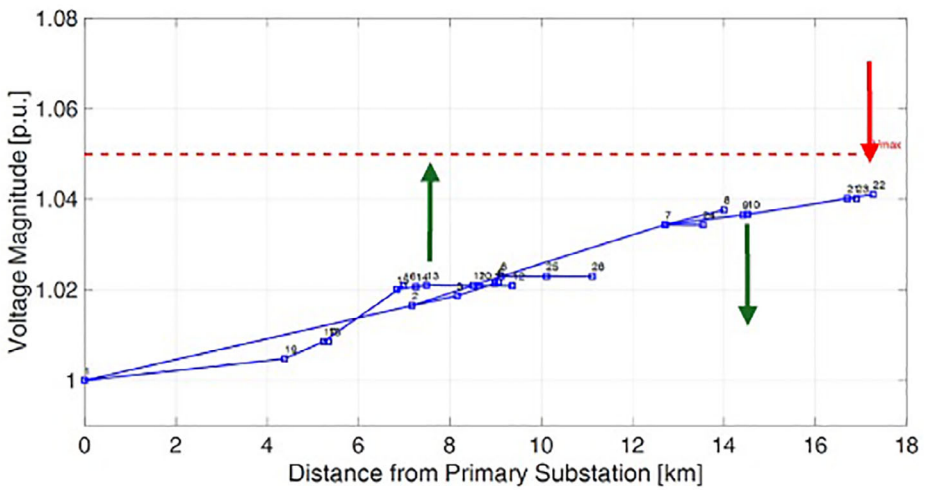

FIGURE 7 | Voltage profile correction at 14:00 by curtailing generation at node 22, together with the downward service and reactive support delivered by the SOP.

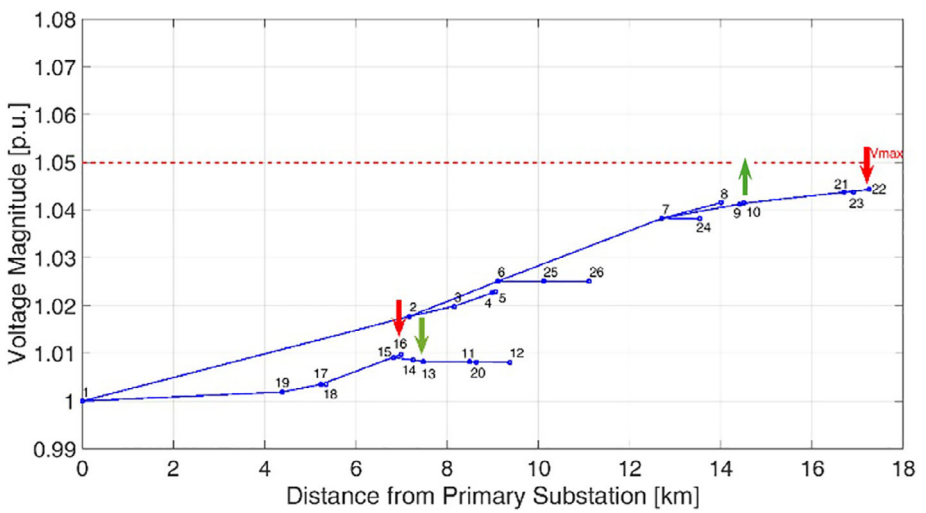

FIGURE 8 | Voltage profile correction at 14:00 by curtailing generation at nodes 22 and 16, and with active and reactive support provided by the SOP.

TABLE 5 | Flexibility exploitation and SOP operation with technical violations in both feeders.

Flexibility resources		12:00	13:00	14:00	15:00	16:00
GC	PV_{16}	—	1%	18%	1%	—
	PV_{22}	—	36%	61%	36%	—
SOP [kW, kVar]	P_{10}^{SOP}	—	−59	−59	−59	—
	P_{13}^{SOP}	—	61	61	61	—
	Q_{10}^{SOP}	146	483	483	483	144
	Q_{13}^{SOP}	263	483	483	483	263

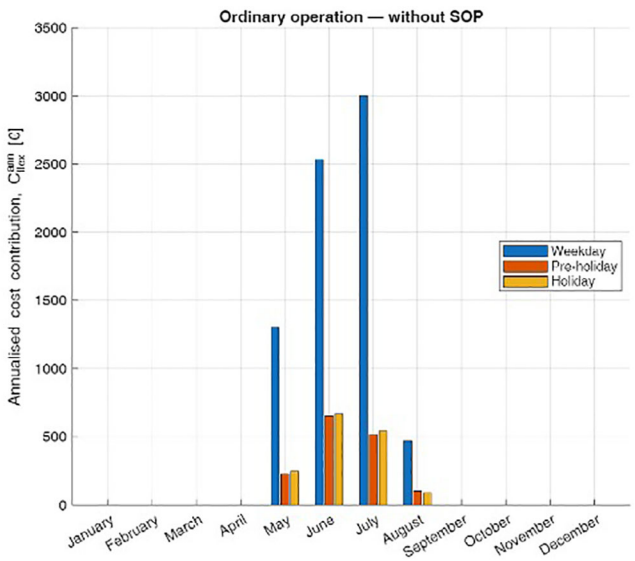

FIGURE 9 | Ordinary operation (without SOP): annualised flexibility procurement cost C_{flex}^{ann} by month and day type (weekday, pre-holiday, and holiday).

Through its operation, the SOP enables the sharing of residual capacity in adjacent feeders, achieving a twofold advantage: reducing flexibility in procurement costs and increasing the distribution network's hosting capacity.

6.2 | Case B – Ordinary Operation Across the Year (Without vs With Coordinated Multi-SOP)

The full-year simulations for Case B show a strongly seasonal pattern in the analysed MV system. Figures 9 and 10 report the annualised flexibility cost indicator C_{flex}^{ann} by month and day type for ordinary operation, distinguishing between the configurations without and with SOP, respectively. Each bar is the contribution to the annual cost, i.e., the representative-day cost multiplied by the number of occurrences in that month/day type.

In the baseline case, the need for corrective actions is concentrated in late spring and summer, with non-zero procurement essentially occurring between May and August. Outside this window, the operating points remain feasible without requiring flexibility activation, indicating that voltage and branch constraints are naturally satisfied under typical demand and generation conditions. This seasonal behaviour is consistent with the

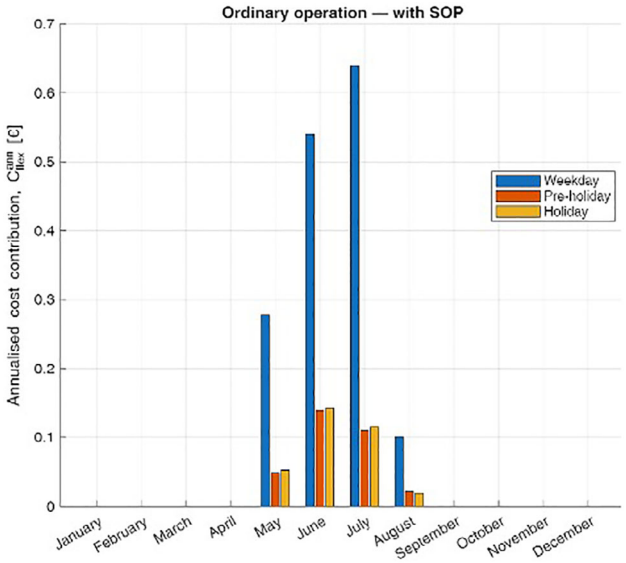

FIGURE 10 | Ordinary operation (with SOP): annualised flexibility procurement cost C_{flex}^{ann} by month and day type (weekday, pre-holiday, and holiday).

expected operating regime of rural MV feeders with high PV penetration: during high-irradiation hours, net injections increase while demand remains comparatively low, resulting in voltage rises in remote sections and, in some instances, reverse-flow patterns that reduce voltage controllability. Figure 9 also shows that the magnitude of flexibility procurement depends on the day type, with weekdays typically driving the largest C_{flex}^{ann} values in the critical months, whereas pre-holiday and holiday profiles yield systematically lower costs. This reflects the interaction between PV production and load shapes: when midday demand is lower relative to PV availability, voltage increases are more pronounced, and mitigation requires stronger corrective actions.

Comparing Figures 9 and 10, enabling SOPs produces a drastic reduction C_{flex}^{ann} during months when violations occur, across all day types.

From a system perspective, SOPs do not "replace" flexibility resources; instead, they expand the set of electrically effective control actions available to the optimiser. Without SOP, constraint relief mainly occurs through local active-power curtailment at PV buses, which directly reduces net injection and alleviates overvoltage. With SOPs, the optimiser can instead utilise inter-feeder coupling and converter-based reactive support to adjust power flows and voltage profiles. Practically, SOPs allow surplus power to be transferred away from the most critical feeder sections and enable local reactive power absorption where voltage sensitivity is highest, thereby restoring voltage regulation while maintaining renewable generation.

6.3 | Case B – N − 1 Assessment Across the Year

While the steady-state operation results quantify how flexibility is utilised to keep the network within limits under forecasted operating conditions, the N − 1 assessment addresses the security-oriented question: how much flexibility must be secured ex ante

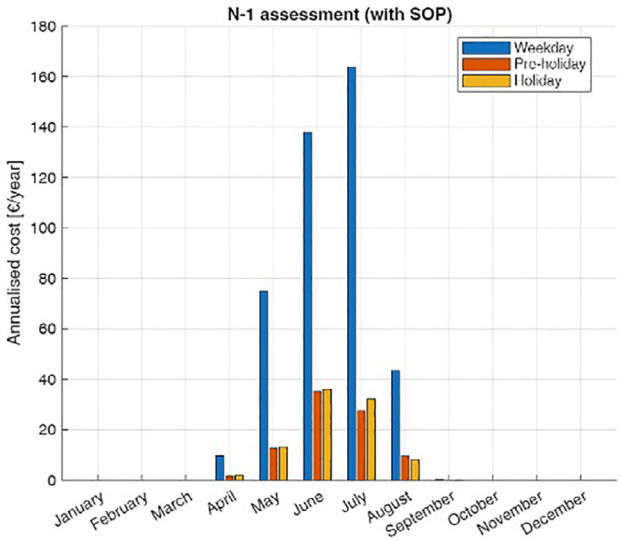

FIGURE 11 | N – 1 assessment (with SOP): annualised contribution to procurement cost by month and day type (weekday, pre-holiday, holiday).

to remain feasible under single-branch outages, given the adopted restoration logic. Figure 11 reports the annualised procurement cost obtained from the N − 1 analysis (with SOP), again split by month and day type. The seasonal footprint remains clearly visible, with the most demanding periods still concentrated in late spring and summer. However, procurement levels increase compared to ordinary operation, reflecting two complementary mechanisms.

First, contingencies modify the post-fault topology and therefore the electrical "shape" of the supplied network. Depending on the fault location and the restoration decision, the supplied portion may exhibit reduced margins, different load-generation distributions, and altered voltage sensitivity patterns, making network operation more demanding even when SOPs remain available. Second, procurement is defined through a security envelope: for each relevant flexibility product, the contracted requirement is taken as the maximum activation observed across the set of analysed contingencies. This worst-case principle naturally yields a more conservative requirement than typical operating points, and it is precisely the output needed for procurement planning rather than for real-time operation. The combined effect is that the annual N − 1 costs preserve the same seasonality as in the ordinary case but amplify it in magnitude, especially in months where PV-induced voltage rise is already a limiting factor.

6.4 | Representative Critical Case

To provide a physical interpretation of the annual results, this subsection focuses on a weekday in July, which falls within the most critical seasonal window and represents a typical condition in which PV-driven overvoltage constraints become binding. The discussion focuses on the peak irradiation hour of 14:00, when the voltage rise is most pronounced. Unlike a time-series depiction, the voltage profiles are displayed along the feeders as a function of distance from the PS, directly revealing the spatial structure of the constraint violations and the impact of corrective actions.

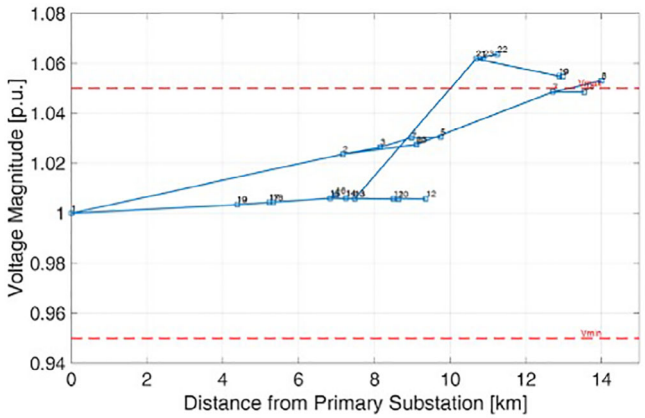

FIGURE 12 | Voltage profiles along the two feeders at 14:00 on a weekday in July.

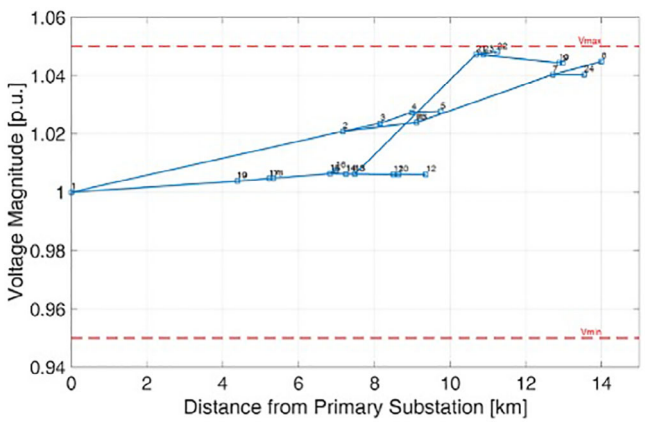

FIGURE 13 | Voltage profile correction at 14:00 by curtailing generation at node 22.

In the base (pre-dispatch) condition, the voltage profile along the feeders exhibits the classical overvoltage pattern of high-PV MV networks: voltages increase with distance, and the remote sections of the most critical feeder exceed the maximum admissible limit (Figure 12).

When SOPs are not available, PV curtailment is activated at the most electrically effective locations, thereby reducing net injections in the critical feeder and bringing the remote nodes below the voltage limit (Figure 13). In contrast, when SOPs are enabled, the corrected profile (Figure 14) is achieved through a different action: rather than reducing PV injections, the optimiser uses converter-based control to provide voltage support and rebalance feeder conditions through controlled coupling.

The resulting profile satisfies the voltage constraint while preserving renewable generation, and the adjacent feeder remains within admissible limits, indicating that the SOP action effectively shares residual capacity and voltage headroom across feeders without creating new violations.

Figure 15 shows that during the critical hours, the baseline case relies on PV curtailment, while the SOP case depends on SOP reactive operation to keep feasibility. Table 6 demonstrates that both approaches fully eliminate voltage violations: the

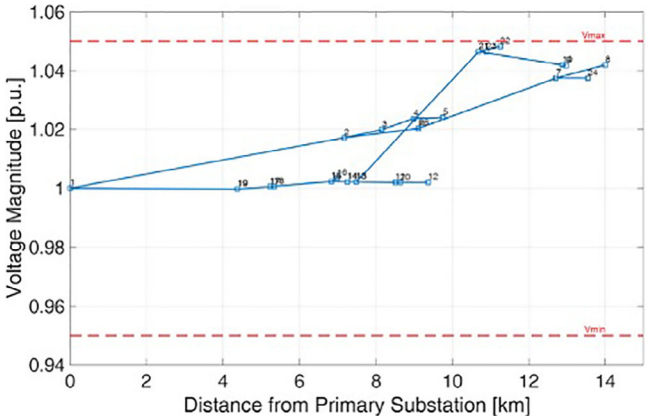

FIGURE 14 | Voltage profile correction at 14:00 with the reactive support delivered by the SOP connected between nodes 21 and 13.

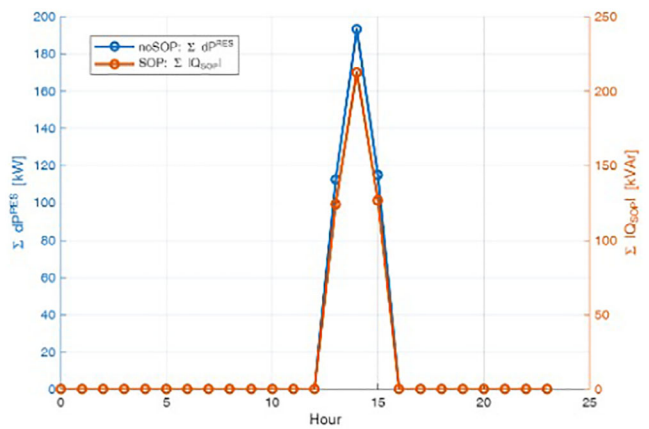

FIGURE 15 | Hourly control action used to restore feasibility (summer weekday): PV curtailment in the baseline case ($\sum dP_{\text{res}}$, without SOP) versus SOP reactive support in the coordinated case ($\sum \mid Q_{\text{sop}} \mid$, with SOP).

TABLE 6 | Key ordinary-operation metrics for the representative case (July – weekday).

Metric	Without SOP	With SOP
Max voltage (base PF) [p.u.]	1.0636	1.0636
Max voltage (after OPF) [p.u.]	1.0489	1.0490
Bus-hours with V > 1.05 (base PF) [#]	13	13
Bus-hours with V > 1.05 (after OPF) [#]	0	0
PV curtailed energy [kWh/day]	421.07	0
Peak PV curtailment [kW]	193.18	0
Peak SOP reactive support [kVAr]	0	212.6
$C_{\text{flex}}^{\text{ann}}$ [€]	3000.95	0.64

maximum voltage drops from 1.0636 p.u. in the base case to about 1.049 p.u. after optimisation, and the total number of violating bus hours drops from 13 to zero. However, the associated cost of feasibility differs radically. Without an SOP, the solution requires a curtailed PV energy of 421.07 kWh/day with a peak curtailment of 193.18 kW. With SOP, curtailed energy and peak curtailment are reduced to zero, while the SOP delivers a peak reactive support of 212.63 kVAr. The annualised contribution $C_{\text{flex}}^{\text{ann}}$ for the July weekday representative case collapses from 3000.95 € (without SOP) to 0.64€ (with SOP). This result is a key practical message: under PV-driven overvoltage, SOP coordination can replace curtailment-based flexibility with converter-based voltage support, leading to near-elimination of renewable curtailment in the most critical operating window of the year.

The N − 1 analysis for the same representative month and day type highlights how security requirements broaden the set of operating conditions the DSO must manage, thereby expanding the control and procurement envelope compared with ordinary operation. Figure 16 summarises this effect by reporting results across all single-branch outages, sorted from the most to the least demanding. In this figure, the horizontal axis represents the position of each contingency in the severity ranking. Two quantities are shown for each ranked outage: (a) the representative-day objective value $f = C_{\text{flex}}^{\text{day}}[€]$ obtained for that contingency; and (b) the corresponding maximum SOP reactive power magnitude $\max_t |Q_{\text{sop}}(t)|$ || kVAr required during the post-contingency corrective action.

As can be seen, the dispersion is substantial. On the one hand, several contingencies are associated with very limited corrective effort (values close to zero), meaning that the post-failure topology remains viable, or can be made viable, without significantly activating flexibility. On the other hand, a significant subset of outages requires significantly more intensive interventions than those observed under normal operating conditions, both in terms of cost and the reactive support required by the SOP. Furthermore, the set of contingencies includes events that cannot be classified as adequate: these are contingencies that create one or more de-energised islands electrically disconnected from any slack/source. Since such islands are not energised after the failure and no switching action or controllable resource is assumed to reactivate them under the recovery logic considered here, they are structurally inadequate, regardless of the SOP control applied to the energised portion of the network.

Table 7 provides a compact quantitative synthesis. Out of 33 analysed outages, eight lead to inadequate conditions due to de-energised islanding. For the remaining adequate contingencies, the distribution of objective values indicates a wide range of post-fault severity: while the minimum is zero, the upper tail reaches $f_{\max} \approx 1.58$ (the representative-day cost) and remains significant at the 95th percentile ($f_{95} \approx 1.35$). This confirms that a procurement strategy calibrated only on typical operating points would underestimate the flexibility needed to ensure secure feasibility across the contingency set. The same conclusion emerges even more clearly from the reactive requirement statistics, which are directly relevant for SOP capability sizing and service contracting. The mean SOP reactive requirement is about 260 kVAr, whereas the upper tail reaches approximately 438.6 kVAr (both as the 95th percentile and as the maximum).

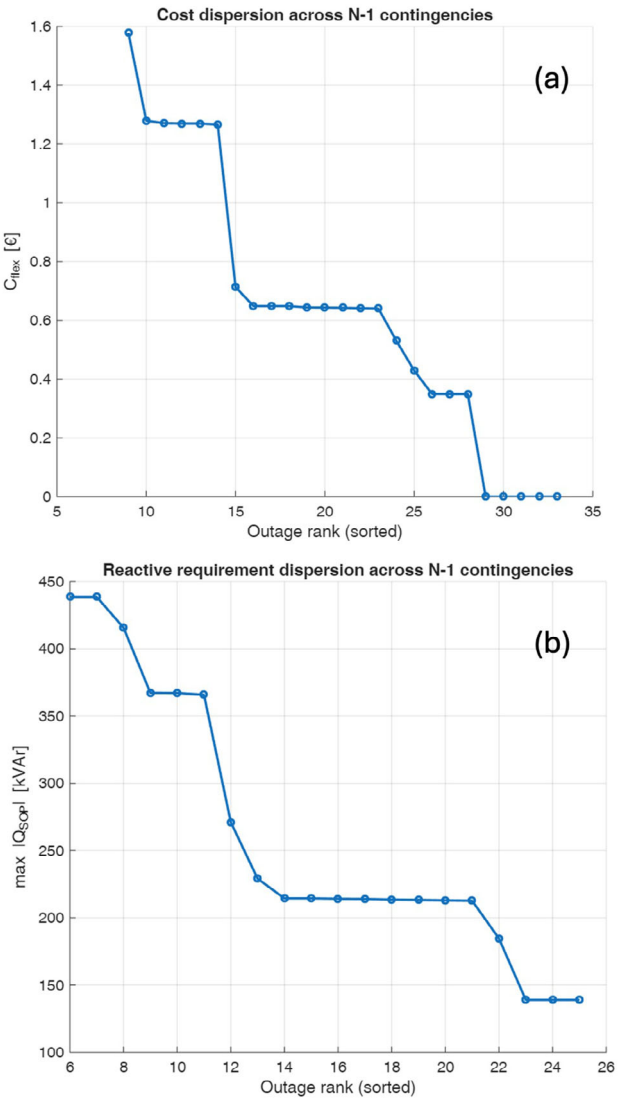

FIGURE 16 | Dispersion across N − 1 contingencies for the representative case, with outages sorted by severity (outage rank). (a) Representative-day objective value $C_{\text{flex}}^{\text{day}}$ [€] for each contingency. (b) Maximum SOP reactive magnitude over the 24-hour profile and across SOP units.

Compared with the ordinary operation peak reactive support of approximately 212.6 kVAr (Figure 17), the N − 1 envelope is roughly twice as large. This is captured by the ratio $Q_{\text{N}-1}/Q_{\text{Ord}} \approx 2.06$ reported in Table 7, which quantifies the additional margin that must be considered when defining SOP reactive capability, or, equivalently, the contracted reactive service to be guaranteed by SOP coordination, if feasibility is to be ensured under N − 1 security conditions.

Overall, the results convey a coherent message across time scales. At the annual level, ordinary-operation procurement is highly seasonal, dominated by PV-induced voltage rise between May and August, with weekdays as the most critical day type. SOP coordination drastically reduces the cost of flexibility procurement in these months by shifting the mitigation strategy from PV curtailment to network-aware converter support. Under N − 1 conditions, the same seasonality persists, but security-driven procurement increases requirements and enlarges the SOP reactive envelope, providing a quantitative basis for sizing and planning decisions. The representative July–weekday analysis makes these mechanisms explicit: without SOP, feasibility is recovered by curtailing PV energy; with SOP, it is achieved through reactive support and inter-feeder balancing, effectively preserving renewable generation while maintaining voltages within technical limits.

TABLE 7 | Key N − 1 metrics for the representative case (July – weekday).

Metric	Value
Number of outages	33
Not adequate contingencies	8
Representative-day objective min value [€]	0
Representative-day objective mean value [€]	0.63
Representative-day objective 95th percentile value [€]	1.35
Representative-day objective max value [€]	1.58
Reactive requirement (mean), $Q_{\text{req,mean}}$ [kVAr]	260.21
Reactive requirement (95th percentile), $Q_{\text{req,95}}$ [kVAr]	438.55
Reactive requirement (max), $Q_{\text{req,max}}$ [kVAr]	438.55
Ratio N − 1 to ordinary (reactive peak), $Q_{\text{N}-1}/Q_{\text{Ord}}$	2.0625

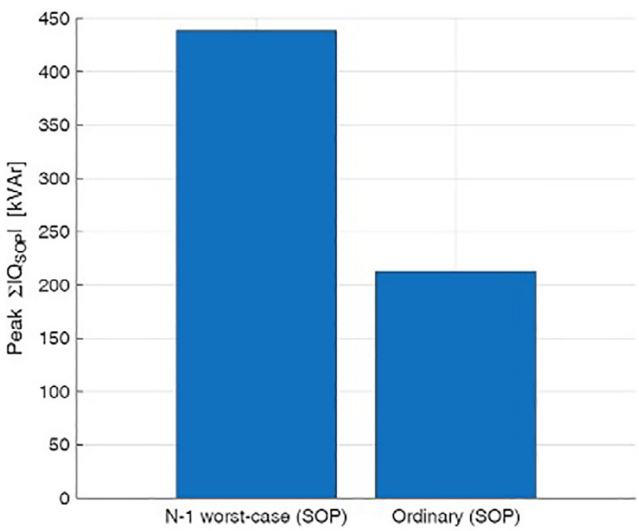

FIGURE 17 | Comparison between the peak reactive support required in the N − 1 worst-case contingency and the peak reactive support required in ordinary operation (SOP-enabled) for the representative case (July – weekday).

6.5 | Computational Scalability and Approximation Accuracy

The proposed methodology was implemented in Python using the scipy.optimize.linprog solver with the HiGHS backend. PF

calculations are executed through external calls to the OpenDSS open-source tool. All simulations were carried out on a standard laptop equipped with an Intel Core i7 processor and 16 GB RAM, without parallelisation.

For the 25-bus case study, the complete 24-hour LP workflow, including PF calculation, hourly sensitivity-matrix evaluation, LP assembly, and optimisation, requires approximately 10–12 s for the normal operating configuration. The $N-1$ analysis for one typical daily profile requires approximately 225–300 s. Extending the procedure to the full set of 36 profiles results in an annual ordinary-operation runtime of 6–8 min, whereas the corresponding annual $N-1$ assessment remains within a few hours. More than 35% of this time is spent on calls to the OpenDSS external tool.

To characterise how computation time scales with network size, the same formulation was also tested on a larger 93-bus MV network with two SOPs, using identical solver settings. In this case, the single 24-hour LP runtime increases to approximately 105 s, compared to approximately 10 s for the 25-bus case. This increase reflects the dominant contribution of sensitivity-matrix construction and LP assembly, whose dimensions grow more than linearly with network size.

The implementation of the PF calculation within the Python-developed tool, the full re-engineering and optimisation of the software, and its parallelisation will drastically reduce this computational time, confirming the practical tractability of the proposed LP-based framework for operational planning applications.

The polygon approximation parameter l affects both the size of the LP problem and the fidelity with which the SOP capability region is represented. To characterise this trade-off and validate the choice $l = 24$, the parameter l was varied over the set {4, 6, 8, 12, 16, 24, 32, 48, 64, 128} in Cases A and B, as well as in the 93-bus scalability benchmark, considering two SOP ratings (1 MVA and 0.2 MVA). Two performance indicators were monitored: the relative error on the optimal cost (f^*) with respect to the $l = 128$ reference solution, defined as

$$\varepsilon(l) = \frac{|f^*(l) - f^*(128)|}{f^*(128)} \times 100\%$$

and the total computation time for a single 24-hour LP run. The results are reported in Figure 18.

Figure 18a shows that the convergence behaviour depends strongly on whether the SOP capability limit is active at the optimum. In the non-saturated situation, i.e., when the SOP rating is sufficiently large relative to the network requirements (1 MVA), the capability constraint is not binding, and the exact shape of the feasible region has little influence on the optimal solution. In this case, the cost error becomes negligible already for small values of l; for the Case B configuration with 1 MVA SOPs, for example, the optimal cost is unchanged for all $l \geq 6$, and this case is therefore omitted from the figure for readability. By contrast, when the SOP operates close to its rated capability (0.2 MVA), the optimum lies on the boundary of the feasible region, and the approximation error decreases much more slowly

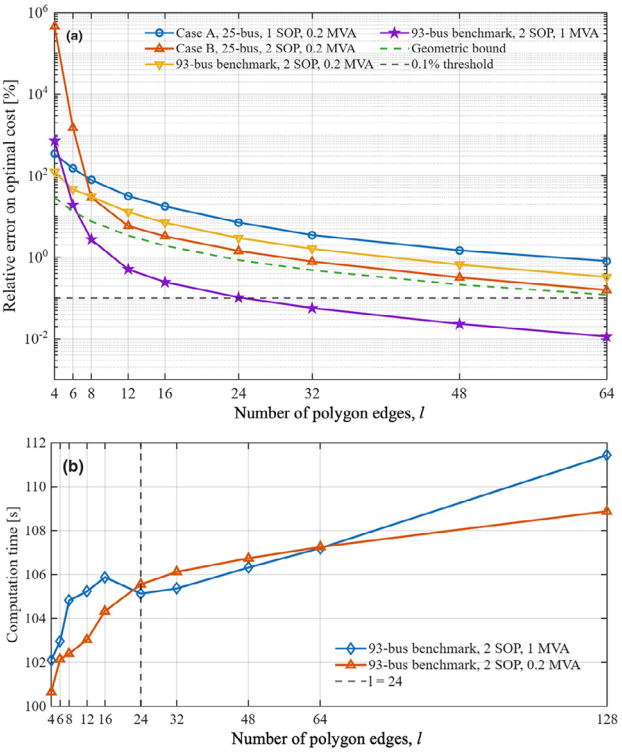

FIGURE 18 | Sensitivity of the LP solution to the number of polygon sides l used to linearise the SOP capability constraint. (a) Relative error on the optimal cost $\varepsilon(l)$ with respect to the $l = 128$ reference solution. The dashed grey curve denotes the geometric approximation bound $\varepsilon_{\text{geom}}$, while the dashed horizontal line indicates the 0.1% accuracy threshold. (b) Total computation time per 24-hour LP run as a function of l for the 93-bus network.

with l. In these saturated cases, coarse polygons may yield overly pessimistic (higher) cost values by excluding feasible operating points that satisfy the true circular capability constraint. This effect is particularly evident for very small values of l (4, 6, and 8 edges), which should therefore be avoided in practical applications.

Figure 18a also shows that, in the saturated cases, the relative cost error may substantially exceed the purely geometric approximation bound, $\varepsilon_{\text{geom}}$, indicating that geometric accuracy alone is not a reliable predictor of the optimal cost's accuracy. In the non-saturated situation, the reverse can be observed: the cost error falls below the geometric bound because the optimum lies in the interior of the capability region, where deviations in the boundary shape have little influence on the objective value.

This is relevant for planning applications, since even modest geometric deviations in the representation of the SOP capability region may translate into appreciable differences in the optimal flexibility procurement cost when the solution is boundary-constrained.

The effect of l on computation time is illustrated in Figure 18b for the 93-bus benchmark, where LP assembly and solution dominate the total runtime and therefore make the dependence on l clearly visible. By contrast, for the 25-bus network, the nearly constant OpenDSS overhead masks most of the LP scaling with l, and

the corresponding timing curves are therefore not reported. For the larger network, the time increases only moderately over the explored range of l, showing that the additional effort associated with finer polygonal approximations is relatively limited.

Overall, these results indicate that the assumption $l = 24$ represents a reasonable default compromise between model size and approximation accuracy for the class of applications considered in this work. It provides very high accuracy when the SOP capability constraint is non-binding or only mildly active while maintaining a limited computational burden. However, when SOP operation is expected to remain persistently close to the capability boundary, a finer approximation, e.g., $l \geq 48$, is preferable to keep the cost error at a low level.

7 | Conclusion

Distribution systems are undergoing a rapid transformation driven by the energy transition, with increasing DER penetration and a growing share of operating points approaching technical limits. In this context, flexibility provisioning is becoming a structural component of DSO operational planning, not only to manage everyday constraint violations but also to guarantee acceptable security margins under credible contingencies.

This paper has presented a practical operational planning framework that quantifies, in a procurement-oriented manner, the flexibility and SOP control effort required to maintain technical feasibility in MV networks. Two deployment scales were analysed on the same physical system: a single-SOP configuration used to highlight the physical mechanism of feeder coupling, and a coordinated multi-SOP configuration used to quantify annual benefits and derive security-driven requirements. In ordinary operation, the results confirm a strongly seasonal pattern of constraint violations in PV-intensive feeders, concentrated in late spring and summer. SOP coordination changes the dominant mitigation strategy: instead of relying primarily on curtailment-based flexibility, feasibility can be restored through electrically efficient converter actions, most notably reactive support at sensitive locations and, when headroom exists, controlled inter-feeder balancing, thereby substantially reducing renewable curtailment during the critical high-irradiance window.

From a security perspective, the N − 1 assessment shows that planning based on typical operating points would underestimate the control envelope required for robust feasibility. When procurement is defined through a worst-case envelope across single-branch outages under a conservative restoration policy, the required SOP reactive capability increases significantly; in the representative critical condition, the peak reactive requirement is approximately doubled compared with ordinary operation. The screening also highlights that a subset of contingencies remains structurally non-restorable under the adopted assumptions because they create de-energised islands electrically disconnected from any supply source; these cases should be interpreted as interrupted-load events rather than as a limitation of the optimisation model.

Overall, the proposed framework provides DSOs with transparent, quantitative indicators to support evidence-based assessments of SOP deployment and flexibility contracting under both operational and security constraints, avoiding reliance on purely deterministic typical-day evaluations. Future work will extend the tool by integrating additional controllable resources and restoration options, such as storage, alternative switching schemes, and explicit re-energisation assumptions for isolated sections, within a comprehensive distribution planning workflow.

Author Contributions

Gianni Celli: conceptualisation, methodology, validation, writing – review & editing, project administration. **Sara Carcangiu:** methodology, software, validation, formal analysis, writing – original draft. **Mansoor U.M. Parehar:** investigation, writing – original draft. **Fabrizio Pilo:** funding acquisition, writing – review & editing.

Acknowledgements

This work was founded by the Research Fund for the Italian Electrical System through the project "Accordo di Programma 2025–2027 – Project 2.3a" between ENEA and the Ministry of the Environment and Energetic Safety (MASE), CUP I53C24003400001. It was also developed within the project funded under the National Recovery and Resilience Plan (NRRP), Mission 4 Component 2 Investment 1.3 – Call for tender No. 1561 of 11.10.2022 of Ministero dell'Università e della Ricerca (MUR), funded by the European Union–NextGenerationEU. Award Number: Project code PE0000021, Concession Decree No. 1561 of 11.10.2022 adopted by Ministero dell'Università e della Ricerca (MUR), CUP F53C22000770007, Project title "Network 4 Energy Sustainable Transition–NEST".

Open access publishing facilitated by Universita degli Studi di Cagliari, as part of the Wiley - CRUI-CARE agreement.

Conflicts of Interest

The authors declare no conflicts of interest.

Data Availability Statement

The data supporting the findings of this study are available upon request from the corresponding author. The data are not publicly available due to privacy or ethical restrictions.

References

1. F. D. Martín, M. Hable, R. Bessa, J. Lassila, C. Imboden, and A. Krula, CIRED Working Group 2019-3, Final Report "Flexibility in active distribution systems," Jan. 2021, http://www.cired.net/cired-working-groups/flexibility-in-active-distribution-systems-wg-2019-3.

2. G. Celli, G. Pisano, S. Ruggeri, et al., "Distribution Systems as Catalysts for Energy Transition Embedding Flexibility in Large-Scale Applications," *IEEE Access* 12 (2024): 92227–92240, https://doi.org/10.1109/ACCESS.2024.3421615.

3. S. Li, Z. Li, M. Shahidehpour, W. Huang, and J. H. Zheng, "Dispatchable Region for Distributed Renewable Energy Generation in Reconfigurable AC–DC Distribution Networks With Soft Open Points," *Applied Energy* 371 (2024): 123704, https://doi.org/10.1016/j.apenergy.2024.123704.

4. C. Heinrich and H. Schmitt, "Integration of New Switching Technologies in Medium-Voltage Systems," in *Proceedings of IEEE International Conference and Exhibition on Electricity Distribution*, London, UK (2001), 1–6, https://doi.org/10.1049/cp:20010866.

5. X. Jiang, Y. Zhou, W. Ming, P. Yang, and J. Wu, "An Overview of Soft Open Points in Electricity Distribution Networks," *IEEE Transactions on Smart Grid* 13, no. 3 (May 2022): 1899–1910, https://doi.org/10.1109/TSG.2022.3148599.

6. K. S. Fuad, H. Hafezi, K. Kauhaniemi, and H. Laaksonen, "Soft Open Point in Distribution Networks," *IEEE Access* 8 (2020): 210550–210565, https://doi.org/10.1109/ACCESS.2020.3039552.

7. W. Cao, J. Wu, N. Jenkins, C. Wang, and T. Green, "Benefits Analysis of Soft Open Points for Electrical Distribution Network Operation," *Applied Energy* 165 (Mar. 2016): 36–47, https://doi.org/10.1016/j.apenergy.2015.12.022.

8. C. Long, J. Wu, L. Thomas, and N. Jenkins, "Optimal Operation of Soft Open Points in Medium Voltage Electrical Distribution Networks With Distributed Generation," *Applied Energy* 184 (Dec. 2016): 427–437, https://doi.org/10.1016/j.apenergy.2016.10.031.

9. R. de Oliveira, L. W. de Oliveira, and E. J. de Oliveira, "Optimization Approach for Planning Soft Open Points in a MV-Distribution System to Maximize the Hosting Capacity," *Energies* 16, no. 3 (Jan. 2023): 1035, https://doi.org/10.3390/en16031035.

10. T. T. Nguyen, T. T. Nguyen, and H. P. Nguyen, "Optimal Soft Open Point Placement and Open Switch Position Selection Simultaneously for Power Loss Reduction on the Electric Distribution Network," *Expert Systems with Applications* 238 (Mar. 2024): 121743, https://doi.org/10.1016/j.eswa.2023.121743.

11. M. Deakin, I. Sarantakos, D. Greenwood, J. Bialek, P. C. Taylor, and S. Walker, "Comparative Analysis of Services From Soft Open Points Using Cost–Benefit Analysis," *Applied Energy* 333 (2023): 120618, https://doi.org/10.1016/j.apenergy.2022.120618.

12. H. Zhan, C. Jiang, and J. Lin, "A Novel Dynamic Reconfiguration Approach for Active Distribution Networks With Soft Open Points and Energy Storage Systems," *Energy Reports* 13 (2025): 1875–1887, https://doi.org/10.1016/j.egyr.2025.01.011.

13. M. Ehsanbakhsh and M. S. Sepasian, "Simultaneous Siting and Sizing of Soft Open Points and the Allocation of Tie Switches in Active Distribution Network Considering Network Reconfiguration," *IET Generation, Transmission & Distribution* 17, no. 1 (2023): 263–280, https://doi.org/10.1049/gtd2.12683.

14. A. Farzamnia, S. Marjani, S. Galvani, and K. T. T. Kin, "Optimal Allocation of Soft Open Point Devices in Renewable Energy Integrated Distribution Systems," *IEEE Access* 10 (Jan. 2022): 9309–9320, https://doi.org/10.1109/ACCESS.2022.3144349.

15. R. You and X. Lu, "Voltage Unbalance Compensation in Distribution Feeders Using Soft Open Points," *Journal of Modern Power Systems and Clean Energy* 10, no. 4 (July 2022): 1000–1008, https://doi.org/10.35833/MPCE.2021.000565.

16. M. Deakin, P. C. Taylor, J. Bialek, and W. Ming, "Design and Operation of Hybrid Multi-Terminal Soft Open Points Using Feeder Selector Switches for Flexible Distribution System Interconnection," *Electric Power Systems Research* 212 (2022): 108516, https://doi.org/10.1016/j.epsr.2022.108516.

17. C. Lou, J. Yang, E. Vega-Fuentes, N. K. Meena, and L. Min, "Multi-Terminal Phase-Changing Soft Open Point SDP Modeling for Imbalance Mitigation in Active Distribution Networks," *International Journal of Electrical Power & Energy Systems* 142 (2022): 108228, https://doi.org/10.1016/j.ijepes.2022.108228.

18. W. Ma, D. Tang, M. Dong, H. Arasteh, and J. M. Guerrero, "Coordinated Robust Configuration of Soft Open Point and Energy Storage Systems for Resilience Enhancement of Integrated Multi-Energy System at Ports," *Applied Energy* 401 (2025): 126644, https://doi.org/10.1016/j.apenergy.2025.126644.

19. C. Han, R. R. Rao, and S. Cho, "Stochastic Operation of Multi-Terminal Soft Open Points in Distribution Networks With Distributionally Robust Chance-Constrained Optimization," *IEEE Transactions on Sustainable Energy* 16, no. 1 (Jan. 2025): 81–94, https://doi.org/10.1109/TSTE.2024.3431616.

20. H. Diao, P. Li, K. Liu, J. Xiao, and Z. Mao, "Co-Deployment of Energy Storage Systems and Soft Open Points in Distribution Networks Considering Normal and Extreme Conditions," *Journal of Energy Storage* 125 (2025): 116806, https://doi.org/10.1016/j.est.2025.116806.

21. J. Li, Y. Zhang, C. Lv, G. Liu, Z. Ruan, and F. Zhang, "Coordinated Planning of Soft Open Points and Energy Storage Systems to Enhance Flexibility of Distribution Networks," *Applied Sciences* 14, no. 18 (2024): 8309, https://doi.org/10.3390/app14188309.

22. C. Wang, J. Sun, M. Huang, X. Zha, and W. Hu, "Two-Stage Optimization for Active Distribution Systems Based on Operating Ranges of Soft Open Points and Energy Storage System," *Journal of Modern Power Systems and Clean Energy* 11, no. 1 (Jan. 2023): 66–79, https://doi.org/10.35833/MPCE.2022.000303.

23. L. Lan, G. Liu, S. Zhu, M. Hou, and X. Liu, "Fault Recovery Strategy for Urban Distribution Networks Using Soft Open Points," *Energy Conversion and Economics* 5, no. 1 (2024): 42–53, https://doi.org/10.1049/enc2.12109.

24. D. Chen, J. Shi, and T. Guan, "Multi-Source Coordinated Fault Recovery Strategy for Flexible Distribution Networks With SOP," in *Proceeding of 2025 International Conference Electrical Automation and Artificial. Intelligence (ICEAAI)* (2025), https://doi.org/10.1109/ICEAAI64185.2025.10956306.

25. M. A. Saaklayen, X. Liang, S. O. Faried, L. Martirano, and P. E. Sutherland, "Soft Open Point-Based Service Restoration Coordinated With Distributed Generation in Distribution Networks," *IEEE Transactions on Industry Applications* 60, no. 2 (March–April 2024): 2554–2566, https://doi.org/10.1109/TIA.2023.3332584.

26. X. Yang, C. Xu, J. Wen, et al., "Cooperative Repair Scheduling and Service Restoration for Distribution Systems With Soft Open Points," *IEEE Transactions on Smart Grid* 14, no. 3 (May 2023): 1827–1842, https://doi.org/10.1109/TSG.2022.3208884.

27. X. Yang, Z. Zhou, Y. Zhang, et al., "Resilience-Oriented Co-Deployment of Remote-Controlled Switches and Soft Open Points in Distribution Networks," *IEEE Transactions on Power Systems* 38, no. 2 (March 2023): 1350–1365, https://doi.org/10.1109/TPWRS.2022.3176024.

28. S. Carcangiu, G. Celli, M. U. M. Parehar, and F. Pilo, "Adoption of Soft Open Points for Increasing the Flexibility Perimeter Exploitation on Power Distribution Networks," in *Proceedings of International Conference and Exhibition on Electricity Distribution (CIRED)* (2025), 3238–3242, https://doi.org/10.1049/icp.2025.2296.

29. G. Celli, M. Galici, and F. Pilo, "Distribution System Planning With Models of Flexibility Markets," in *27th International Conference on Electricity on Electricity Distribution (CIRED 2023)* (2023), 3996–4003, https://doi.org/10.1049/icp.2023.0495.